Multi-vortex crystal lattices in Bose-Einstein Condensates with a rotating trap

Shuangquan Xie, Panayotis G. Kevrekidis and Theodore Kolokolnikov

August 16, 2017

Abstract

We consider vortex dynamics in the context of Bose-Einstein Condensates (BEC) with a rotating trap, with or without anisotropy. Starting with the Gross-Pitaevskii (GP) partial differential equation (PDE), we derive a novel reduced system of ordinary differential equations (ODEs) that describes stable configurations of multiple co-rotating vortices (vortex crystals). This description is found to be quite accurate *quantitatively* especially in the case of multiple vortices. In the limit of many vortices, BECs are known to form vortex crystal structures, whereby vortices tend to arrange themselves in a hexagonal-like spatial configuration. Using our asymptotic reduction, we derive the effective vortex crystal density and its radius. We also obtain an asymptotic estimate for the maximum number of vortices as a function of rotation rate. We extend considerations to the anisotropic trap case, confirming that a pair of vortices lying on the long (short) axis is linearly stable (unstable), corroborating the ODE reduction results with full PDE simulations. We then further investigate the many-vortex limit in the case of strong anisotropic potential. In this limit, the vortices tend to align themselves along the long axis, and we compute the effective one-dimensional vortex density, as well as the maximum admissible number of vortices. Detailed numerical simulations of the GP equation are used to confirm our analytical predictions.

1 Introduction

Theoretical and experimental studies on vortices in rotating Bose-Einstein Condensates (BEC) have attracted great interest in the past 20 years, see, e.g. [1], the review [2] and the monographs [3, 4] where extensive lists of references can be found. In most of the theoretical research, the Gross-Pitayevskii equation (GPE) model has served to study the emergence and dynamics of vortices. As an approximation of the quantum mechanical many-body problem at zero temperature, Gross-Pitaevskii theory was rigorously established in [5] for the non-rotating case and in [6] for rotating systems.

One of the most interesting features observed experimentally is that when the angular speed gets larger, vortices are spontaneously nucleating [2], since their presence minimizes the system's free energy. As the frequency of rotation is increased, the number of vortices increases and they eventually arrange themselves in a hexagonal lattice-like pattern around the center of the condensate [7, 8]. It is natural to explore the mechanism of this behavior mathematically. Under the framework of GP theory, the critical angular velocity was rigorously computed in [9, 10] and the distribution of the first few vortices to appear in the condensate was studied in [11]. Another striking observation in experiments is that the vortex lattice seems to be nearly homogeneous even when the matter density profile of the condensate imposed by the trap is not homogeneous [12, 13]. The relation between the matter density and the vortex density has been formulated in [14, 15]. However, Ref. [16] argues that the vortex distribution is strongly inhomogeneous close to the critical speed for vortex nucleation and gradually homogenizes when the rotation speed is increased. The study of both such vortex lattices and also of small scale vortex clusters [17, 18], thus, remains an active topic of both theoretical and experimental investigation.

In this paper, we use asymptotic techniques following [19] to derive a novel set of equations which describe

the distribution of vortex lattices in rotating BEC [1]. The equations we derive are valid for both the isotropic and the anisotropic case. We then use the new equations to study the following important limits:

- **Many-vortex limit, isotropic trap:** This is the limit where vortex crystals are observed. By taking a continuum limit of the effective equations of motion, we consider the equilibrium of the effective density of the vortex crystals, as well as the size of the lattice. In addition, this computation yields an asymptotic estimate for the *maximum* number of vortices that can form stable lattice configurations, as a function of rotation speed. This is illustrated in Figure 1.

- **High anisotropy many-vortex regime:** When the anisotropy is sufficiently high, the vortices tend to align along the longer axis of the trap; see Figure 5. This constitutes the energetically favorable configuration. In this limit, we compute the one-dimensional density of the resulting vortex configuration by using techniques involving the Chebyshev polynomials. As in the isotropic case, this leads to an expression relating the maximum number of vortices in a stable configuration and other problem parameters such as the anisotropy and the rotation rate.

We validate our results by a direct comparison of the reduced particle ODEs with the full numerical solution. The PDE system is simulated using the finite-element package FlexPDE6 [22]. FlexPDE6 uses adaptive mesh in space, and adaptive time stepping. This is particularly useful for computing vortex solutions which are localized in space. In our computations we used up to 40000 nodes with global error tolerances up to 10^{-4}. To validate the numerics we verified that doubling mesh size and error tolerances did not affect the overall results.

Our starting point is the Gross-Pitaevskii (GP) equation with an inhomogeneous rotating trap in two dimensions given by

$$(\gamma - \kappa i)w_t = \Delta w + \frac{1}{\varepsilon^2}\left(V(x) - |w|^2\right)w + i\Omega\left(x_2 w_{x_1} - x_1 w_{x_2}\right). \tag{1a}$$

The parameter ε is assumed to be small, which corresponds to the large chemical potential (also known as semiclassical [4]) limit. Ω is the rotation rate, and $V(x)$ is the trap potential. We consider the general anisotropic parabolic potential [2] $V(x)$,

$$V(x) = 1 - x_1^2 - b^2 x_2^2 \tag{1b}$$

The parameter b represents the strength of the anisotropy, with the isotropic trap limit corresponding to $b = 1$. Here, we use the notation $V = 1 - \tilde{V}$ where $\tilde{V}$ represents the customary confining parabolic trap. Finally, the ratio γ/κ represents the finite temperature effects; see the relevant discussion in [23, 24]. For the purposes of numerical simulations, we mostly work in the the overdamped regime $\gamma/\kappa \to \infty$, sometimes referred to as imaginary time integration [24, 25]. While the equilibrium vortex lattice state is independent of γ, numerical simulations are easier to perform in the overdamped regime. I.e., Our aim from the point of view of numerical computations is to converge to these vortex-filled equilibrium states (shared between the conservative and the dissipative variant of the model), hence we use an unrealistically large value of γ to expedite this convergence.

Let us now summarize the main findings of this paper.

1. **Reduced equations for vortex motion.** In §2 and §2.2 we extend the asymptotic methods first developed in [19] to the case of a rotating trap. The presence of the inhomogeneous trap introduces

---

[1]Admittedly, there are numerous other techniques that enable the derivation of such vortex equations, including the use of conservation laws [20], as well as of variational principles [21]. Here, we focus on the asymptotic techniques of [19].

[2]Note that it is easy to extend to the result to the more general case: $V(x) = 1 - b_1^2 x_1^2 - b_2^2 x_2^2$. In fact, we could just rescale $\hat{t} = \frac{t}{b_1^2}$, $\hat{x}_1 = b_1 x_1$, $\hat{x}_2 = b_1 x_2$ and define $b = \frac{b_2}{b_1}$, $\hat{\varepsilon} = b_1 \varepsilon$, $\hat{\Omega} = \frac{\Omega}{b_1^2}$ so that the PDE (1) becomes:

$$(\gamma - \kappa i)w_{\hat{t}} = \Delta w + \frac{1}{\hat{\varepsilon}^2}\left(1 - \hat{x}_1^2 - b^2 \hat{x}_2^2 - |w|^2\right)w + i\hat{\Omega}\left(\hat{x}_2 w_{\hat{x}_1} - \hat{x}_1 w_{\hat{x}_2}\right).$$
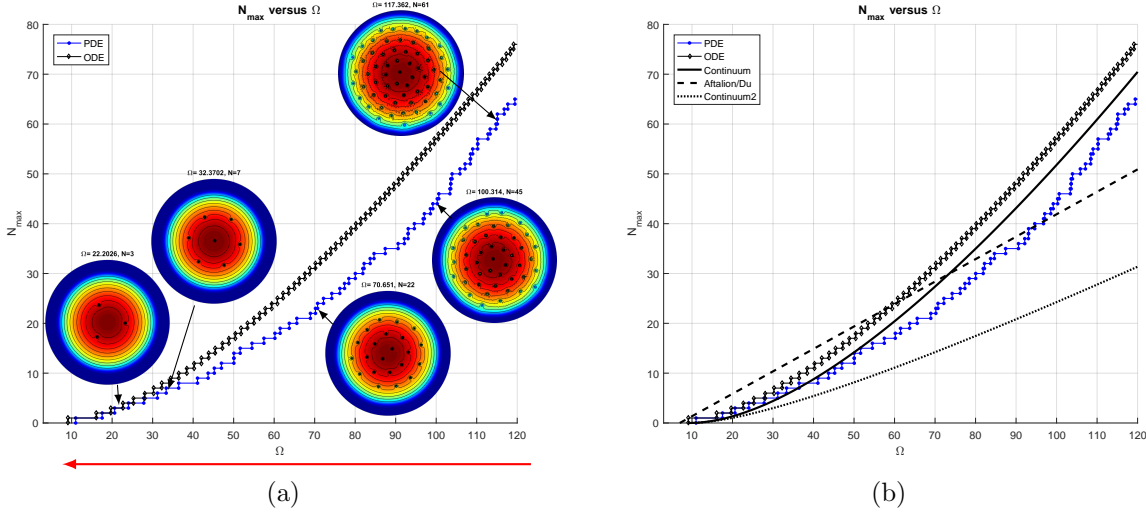
Figure 1: (a) Maximum number of vortices as a function of Ω. "PDE" denotes the full PDE simulation of (1) in the overdamped regime ($\kappa = 0, \gamma = 1$). We start with $\Omega = 125$ and an initial configuration of 80 vortices. Then Ω is decreased very slowly in time according to the formula $\Omega = 125 - 10^{-4}t$ (indicated by a red arrow). Other parameters are $b = 1, \varepsilon = 0.01$. We count the number of vortices at each value of Ω, and this is what is plotted. "ODE" denotes the simulation of the reduced ODE system (2), with the same parameters as the PDE. See remarks following Eq. (53) for further details of PDE/ODE simulations. Snapshots show steady states of the PDE for several values of Ω. (b) Comparison to previous results. "PDE" and "ODE" are the same as in (a). "Continuum" refers to Eq. (4). "Aftalion/Du" is the Eq. (54) originally derived in [26]. Finally, "Continuum2" represents Eq. (56) first derived in [27].

several complications, most notably the inhomogeneous density background on top of which the vortices evolve (and interact). The end result that we obtain through this analysis is the following system for the motion of N vortices whose positions are given by ξ_j, $j = 1 \ldots N$:

$$\gamma \log\left(1/\varepsilon\right)\xi_{jt} + \kappa \xi_{jt}^{\perp} = \left(-\frac{2\Omega}{1+b^2} + \frac{2\log\left(1/\varepsilon\right)}{V(\xi_j)}\right)\begin{pmatrix} 1 & 0 \\ 0 & b^2 \end{pmatrix}\xi_j + 2\sum_{k \neq j}\frac{(\xi_j - \xi_k)}{|\xi_j - \xi_k|^2}\frac{V(\xi_j)}{V(\xi_k)}. \qquad (2)$$

Here and below, we use the notation $(a, b)^{\perp} = (-b, a)$.

We draw the reader's attention to the term $\frac{V(\xi_j)}{V(\xi_k)}$ which modifies the "classical" Helmholtz-type vortex-to-vortex interaction of the form $\xi_{jt}^{\perp} = \sum_{k \neq j}\frac{(\xi_j - \xi_k)}{|\xi_j - \xi_k|^2}$. Equation (2) reduces to the "classical" case (of Hamiltonian point vortex motion) when $V = 1, \gamma = 0$ and $\Omega = 0$, corresponding to a constant trap, no rotation, and no damping. To our knowledge, this is the first time that this additional term has been proposed and it incorporates in a fundamental way the role of the potential (and also of the anisotropy when the latter is present) towards screening the inter-vortex interaction. In [27], the same equation as (2) but without the term $\frac{V(\xi_j)}{V(\xi_k)}$ was used to describe vortex dynamics in BEC. We show that our modified equation (2) agrees with full numerical simulations of the original GPE (1a) much better, particularly in the case of multiple vortices; relevant examples will be considered in Figs. 1, 2.

The remaining results in the paper follow from the analysis of the reduced equation (2).

2. **Large-N vortex lattice density and radius for isotropic potential.** Here, we extend the methods reported in [27] to derive the continuum limit density for the steady state of (2). In §3 we show that

3

in the large-N limit, the radius a of the vortex lattice is related to Ω, N, ε via the formula

$$N \sim \frac{1}{\nu}\left(\left(-1-\frac{1}{2}\Omega\nu\right)\ln(1-a^2)+2-2(1-a^2)^{-1}\right), \quad N \gg 1 \tag{3}$$

where $\nu = 1/\log\left(1/\varepsilon\right)$. See Figure 2, where the asymptotic radius a given by solving (3) is shown in dashed curve, and a good agreement with full numerics is observed.

3. **Maximal admissible number of vortices**. As we show in §3, an immediate consequence of (3) is the existence of a fold-point bifurcation which results in the disappearence of some of the vortices as Ω is decreased, as illustrated in figure 1. Stated differently, for a fixed Ω, there is a maximum $N_{\max}$ such that N-vortex lattice exists if and only if $N \leq N_{\max}$ where

$$N_{\max} = \frac{1}{\nu}\left\{(\Omega\nu+2)\left(\frac{1}{2}\ln(\Omega\nu+2)-\ln(2)-\frac{1}{2}\right)+2\right\}. \tag{4}$$

Figure 1 illustrates this result.

4. **Stability of two vortices in the anisotropic case.** In §4 we study the stability of a two-vortex steady state with respect to the above mentioned ODE dynamics. By symmetry, there are two equilibrium states: the two vortices lying on major or minor axis. However, the equilibrium along the minor axis is unstable [28, 29]. Furthermore, a two vortex-state on the major axis becomes unstable as Ω is decreased due to a fold point bifurcation. We compute this bifurcation and compare this to numerics. In paper [26] a similar threshold was computed for the anisotropic case from the energy point of view; this was also featured in the work of [17] for the isotropic case, connecting the ODEs with the GP PDE and also experimental results.

5. **High anisotropy, large N limit (§5).** Sufficiently high anisotropy "pushes" all the vortices to align along the major axis (see figure 5, as well as [30]; for some case examples with opposite charges see [28]). In the dual limit of high anisotropy and large N, the steady state becomes essentially one-dimensional and we compute the effective one-dimensional density using techniques involving the Chebychev polynomials. As in the radially symmetric case, the vortex "lattice" has a radius a which, in the case $b \ll 1$, is implicitly given via equation

$$N \sim \frac{1}{\nu}\left(\frac{\Omega\nu}{1+b^2}\frac{a^2}{2\sqrt{1-a^2}}-\frac{(a^2-2)^2}{\nu(1-a^2)^{\frac{3}{2}}}+1\right). \tag{5}$$

6 **Maximal admissible number of vortices, high anisotropy (§5).** Finally, as in the radially symmetric anisotropic case, we compute $N_{\max,1d}$, the maximum number of vortices admissible for a given Ω when the anisotropy is sufficiently high to align all vortices along the major axis. It is obatined by maximizing (5) which yields

$$N_{\max,1d} = \frac{1}{\nu}\left(1+3^{-3/2}\left(\frac{\Omega\nu}{1+b^2}-4\right)\sqrt{1+2\frac{\Omega\nu}{1+b^2}}\right), \quad b \ll 1 \tag{6}$$

There have been two approaches to the dynamics of vortices in a trapped condensate. The first approach relies on the fact that GP equation is the Euler-Lagrange equation for the time-dependent Lagrangian functional under variation of the wave function. If one is interested in an effective description for the evolution of the vortex centers and how it varies upon variation of one or more parameters, the resulting Lagrangian functional can be used together with a multi-vortex ansatz to provide approximate Lagrangian equations of motion [1, 31, 26, 32]. Another approach is to study GP equation itself, which is the approach we take herein. Due to the presence of two length scales: the size of vortex core and the inter-vortex distance, it is possible to employ the method of matched asymptotics [19, 33, 34, 35, 36]. This also leads to the derivation of dynamical equations for the evolution of the vortex centers.
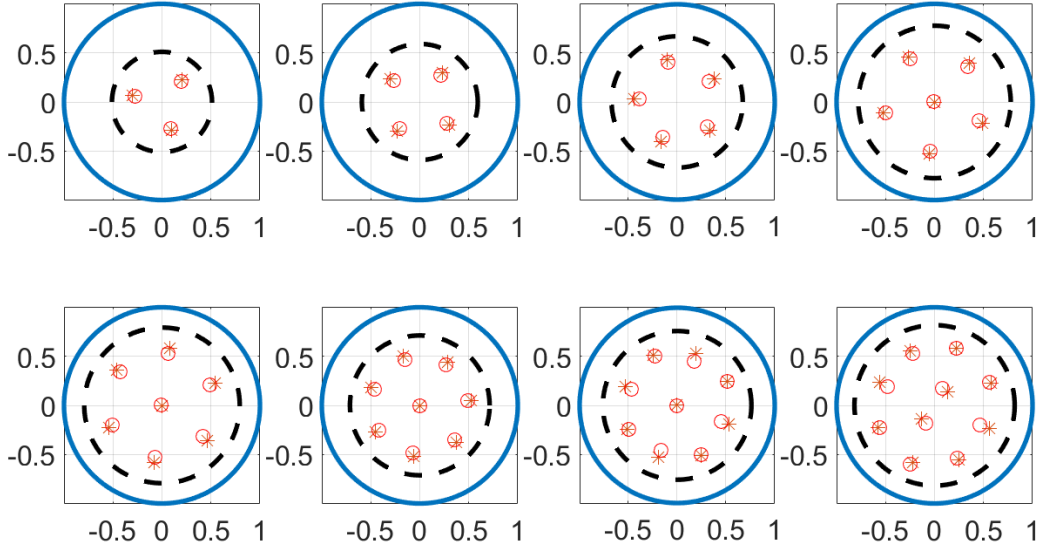
Figure 2: Comparison of the steady state of PDE and ODE simulations. '$*$' denotes the steady state of the ODE system (2) whereas 'o' is from the PDE system (1). The parameters are chosen as: $\gamma = 1$, $\kappa = 0$, $b = 1$, $\varepsilon = 0.025$ and $\Omega = 29.51$ for 3 to 7 vortices and $\Omega = 36.89$ for 8 to 10 vortices. The dashed line represents the radius prediction a from (3).

2   Vortex dynamics

We now derive vortex dynamics for (1a), following closely the exposition of [19]. We start by deriving the dynamics of a single vortex, then expand our calculations to multiple vortices.

2.1   Single vortex

Suppose that the vortex center is located at $\xi = (\zeta, \eta) \in \mathbb{R}^2$. Following [19], we decompose the solution into the outer region $O(\varepsilon)$ away from the vortex center, and the inner region near the vortex center. We will then use matched asymptotics to match the two regions which will yield the equation of motion.

In the outer region, outside the vortex core $|x - \xi| \gg O(\varepsilon)$, we decompose the solution into phase ϕ and amplitude u:

$$w = u e^{i\phi}. \tag{7}$$

Substituting (7) into (1a) and separating the real and imaginary part, we then obtain:

$$\gamma u_t + \kappa u \phi_t = (\Delta u - u|\nabla \phi|^2) + \frac{1}{\varepsilon^2} \left(V(x) - u^2\right) u + \Omega u \phi_\theta \tag{8}$$

$$-\kappa u_t + \gamma u \phi_t = u \Delta \phi + 2\nabla u \cdot \nabla \phi - \Omega u_\theta. \tag{9}$$

We then expand u and ϕ with respect to ε: $u = u_0 + \varepsilon u_1 + \cdots$ and $\phi = \phi_0 + \varepsilon \phi_1 + \cdots$. The leading order equations yield

$$u_0 = \sqrt{V(x)} \tag{10a}$$

and

$$\gamma \phi_{0t} = \Delta \phi_0 + \frac{1}{2} \frac{\nabla V}{V} \cdot \left(2\nabla \phi_0 - \Omega x^\perp\right). \tag{10b}$$

5

Assume that a vortex has charge $+1$, so that ϕ_0 satisfies a point boundary condition

$$\phi_0 \to \arg(x - \xi) \quad \text{as } x \to \xi. \tag{11}$$

In order to match to the inner solution of the vortex inside the vortex core, we need to understand in more detail the local behaviour of the outer solution away from the vortex points. We first decompose ϕ_0 as

$$\phi_0 = S + \tilde{\phi}_0 \tag{12}$$

where S is a regular solution (without any singularities) to

$$0 = \Delta S + \frac{1}{2} \frac{\nabla V}{V} \cdot \left(2 \nabla S - \Omega x^\perp \right). \tag{13}$$

For the elliptic trap (1b), its solution is given by

$$S(x) = \frac{\Omega}{2} \frac{b^2 - 1}{1 + b^2} x_1 x_2. \tag{14}$$

Notice that this contribution vanishes in the isotropic limit of $b = 1$. We change to the moving coordinate $\tilde{x} = x - \xi(t)$ and denote by $(\tilde{r}, \tilde{\theta})$ the polar coordinates in moving coordinate. Then (10b) becomes:

$$\gamma \left(\tilde{\phi}_{0t} - \xi_t \cdot \nabla \tilde{\phi}_0 \right) = \Delta \tilde{\phi}_0 + \frac{\nabla V(\xi + \tilde{x}) \cdot \nabla \tilde{\phi}_0}{V(\xi + \tilde{x})}, \tag{15}$$

or, to leading order,

$$0 \sim \Delta \tilde{\phi}_0 + \left(\gamma \xi_t^\perp + \frac{\nabla^\perp V(\xi)}{V(\xi)} \right) \cdot \nabla \tilde{\phi}_0. \tag{16}$$

where we have assumed that the time-dynamics are sufficiently slow that $\gamma \tilde{\phi}_{0t}$ can be discarded. In particular this is the case near a stable equilibrium.

We now solve (16) iteratively near the singularity $\tilde{x} \to 0$. The leading-order solution must match the point-boundary condition (11) which yields $\tilde{\phi}_0 \sim \tilde{\theta}$. Upon substituting $\tilde{\phi}_0 \sim \tilde{\theta} + \phi_{01}$ we obtain

$$0 = \Delta \phi_{01} + \left(\gamma \xi_t + \frac{\nabla V(\xi)}{V(\xi)} \right) \cdot \left(\frac{\tilde{x}^\perp}{|\tilde{x}|^2} + \nabla \phi_{01} \right). \tag{17}$$

The term $\nabla \phi_{01}$ is of smaller order than the other terms. Formal expansion then yields

$$\phi_{01} = \frac{1}{2} (\log \tilde{r}) \left(\gamma \xi_t^\perp + \frac{\nabla^\perp V(\xi)}{V(\xi)} \right) \cdot \tilde{x}.$$

Finally, at the next iteration we let $\tilde{\phi}_0 \sim \tilde{\theta} + \phi_{01} + \phi_{02}$. This yields $\phi_{02} \sim K \cdot \tilde{x}$ where the vector K depends on the vortex locations and will be determined later via asymptotic matching. In summary, we obtain

$$\phi_0(\tilde{x}, t) = S + \tilde{\theta} + \frac{1}{2} (\log \tilde{r}) \left(\gamma \xi_t^\perp + \frac{\nabla^\perp V(\xi)}{V(\xi)} \right) \cdot \tilde{x} + K \cdot \tilde{x} + \mathcal{O}(\tilde{r}^2 \log \tilde{r}) \tag{18}$$

We now Taylor expand the outer solution as $x \to \xi$. We have

$$e^{i\phi_0} = e^{i(\tilde{\theta} + S(\xi))} \left(\frac{1}{2} (\log \tilde{r}) \left(\gamma \xi_t^\perp + \frac{\nabla^\perp V(\xi)}{V(\xi)} \right) \cdot \tilde{x} + K \cdot \tilde{x} \right) + \mathcal{O}(\tilde{r}^2 \log \tilde{r});$$

$$u_0 = \sqrt{V(\xi)} + \frac{\nabla V(\xi) \cdot \tilde{x}}{2\sqrt{V(\xi)}} + \mathcal{O}(\tilde{r}^2);$$

This yields the following singularity behaviour for w as $x \to \xi$:

$$w(\tilde{x}, t) = e^{i(\tilde{\theta} + S(\xi))}\left(\sqrt{V(\xi)} + \frac{\nabla V(\xi) \cdot \tilde{x}}{2\sqrt{V(\xi)}}\right)\left(1 + \frac{i}{2}(\log \tilde{r})\left(\gamma \xi_t^\perp + \frac{\nabla^\perp V(\xi)}{V(\xi)}\right) \cdot \tilde{x} + i(K + \nabla S) \cdot \tilde{x}\right) + \mathcal{O}(\tilde{r}^2 \log \tilde{r}) + \mathcal{O}(\varepsilon)$$

(19)

Next we consider the inner region, let

$$y = \frac{x - \xi}{\varepsilon}$$

and expand $w = W_0(y) + \varepsilon W_1(y) + \cdots$. In order to match each order of ε, W_0, W_1 must satisfy:

$$0 = \Delta_y W_0 + V(\xi)W_0 - |W_0|^2 W_0 \tag{20}$$

$$\left(-(\gamma - \kappa i)\xi_t + i\Omega\xi^\perp\right) \cdot \nabla_y W_0 - 2\nabla V(\xi) \cdot yW_0 = \Delta_y W_1 + V(\xi)W_1 - |W_0|^2 W_1 - W_0\left(W_0\overline{W_1} + W_1\overline{W_0}\right) \tag{21}$$

We scale out $V(\xi)$ by changing variables

$$z = \sqrt{V(\xi)}y; \quad W_0(y) = \sqrt{V(\xi)}U_0(z), \quad W_1(y) = U_1(z)$$

assuming that ξ is slowly varying (so that it can be considered constant along the scale of variation of y), in which case U_0, U_1 satisfies:

$$0 = \Delta_z U_0 + U_0 - |U_0|^2 U_0 \tag{22}$$

$$\left(-(\gamma - \kappa i)\xi_t + i\Omega\xi^\perp\right) \cdot \nabla_z U_0 - \frac{\nabla V(\xi) \cdot z}{V(\xi)}U_0 = \Delta_y U_1 + U_1 - |U_0|^2 U_1 - U_0\left(U_0\overline{U_1} + U_1\overline{U_0}\right). \tag{23}$$

We look for a vortex solution of U_0 in the form of $U_0(z) = f_0(R)e^{i(\theta + S(\xi))}$, where R, θ denote the polar coordinates of $z = Re^{i\theta}$. Then (22) reduces to

$$f_0'' + \frac{1}{R}f_0' - \frac{1}{R^2}f_0 + f_0(1 - f_0^2) = 0 \tag{24}$$

with the boundary condition:

$$f_0(0) = 0, \quad f_0(+\infty) = 1. \tag{25}$$

The solution to (24, 25) is well known to be unique [37]. The large R expansion shows that f_0 satisfies

$$1 - f_0^2 - 1/R^2 = O(1/R^4), \quad R \to \infty. \tag{26}$$

Let $U_1 = f_1(R, \theta, t)e^{i(\theta + S(\xi))}$. In terms of f_1, (23) becomes:

$$\left(-(\gamma - \kappa i)\xi_t + i\Omega\xi^\perp\right) \cdot (f_0'\nabla_z R + if_0\nabla_z\theta) - \frac{\nabla V(\xi) \cdot z}{V(\xi)}f_0 = \Delta_z f_1 + 2i\left(\nabla_z f_1 \cdot \nabla_z \theta\right) - \frac{1}{R^2}f_1 + f_1(1 - 2f_0^2) - f_0^2\overline{f_1} \tag{27}$$

We then decompose further $f_1 = A(R)\cos\theta + B(R)\sin\theta$ and separate real and imaginary parts:

$$A = A_r + iA_i, \quad B = B_r + iB_i$$

to obtain the following equations for A_r, A_i, B_r, B_i:

$$-\frac{V_{x_1}(\xi)R}{V(\xi)}f_0 - \gamma\zeta_t f_0' - \frac{\Omega\zeta + \kappa\eta_t}{R}f_0 = A_r'' + \frac{1}{R}A_r' + (1 - 3f_0^2 - \frac{2}{R^2})A_r - \frac{2B_i}{R^2} \tag{28}$$

$$-\frac{V_{x_2}(\xi)R}{V(\xi)}f_0 - \gamma\eta_t f_0' - \frac{\Omega\eta - \kappa\zeta_t}{R}f_0 = B_r'' + \frac{1}{R}B_r' + (1 - 3f_0^2 - \frac{2}{R^2})B_r + \frac{2A_i}{R^2} \tag{29}$$

$$\frac{-\gamma\eta_t f_0}{R} - \Omega\eta f_0' + \kappa\zeta_t f_0' = A_i'' + \frac{1}{R}A_i' + (1 - f_0^2 - \frac{2}{R^2})A_i + \frac{2B_r}{R^2} \tag{30}$$

$$\frac{\gamma\zeta_t f_0}{R} + \Omega\zeta f_0' + \kappa\eta_t f_0' = B_i'' + \frac{1}{R}B_i' + (1 - f_0^2 - \frac{2}{R^2})B_i + \frac{2A_r}{R^2}. \tag{31}$$

We are concerned about the behaviour of the solutions of these equations at infinity. As $R \to \infty$, we have:

$$-\frac{V_{x_1}(\xi)R}{V(\xi)}\left(1 - \frac{1}{R^2}\right) - \frac{\Omega\zeta + \kappa\eta_t}{R} = A_r'' + \frac{1}{R}A_r' + (-2 + \frac{1}{R^2})A_r - \frac{2B_i}{R^2} + \mathcal{O}\left(\frac{1}{R^3}\right) \tag{32}$$

$$-\frac{V_{x_2}(\xi)R}{V(\xi)}\left(1 - \frac{1}{R^2}\right) - \frac{\Omega\eta - \kappa\zeta_t}{R} = B_r'' + \frac{1}{R}B_r' + (-2 + \frac{1}{R^2})B_r + \frac{2A_i}{R^2} + \mathcal{O}\left(\frac{1}{R^3}\right) \tag{33}$$

$$\frac{-\gamma\eta_t}{R} = A_i'' + \frac{1}{R}A_i' - \frac{1}{R^2}A_i + \frac{2B_r}{R^2} + \mathcal{O}\left(\frac{1}{R^3}\right) \tag{34}$$

$$\frac{\gamma\zeta_t}{R} = B_i'' + \frac{1}{R}B_i' - \frac{1}{R^2}B_i - \frac{2A_r}{R^2} + \mathcal{O}\left(\frac{1}{R^3}\right). \tag{35}$$

By expressing the solutions in a power series of R and $\log R$ for large R, we obtain

$$A_r = \frac{V_{x_1}(\xi)R}{2V(\xi)} - \left(\frac{\gamma\zeta_t}{2} + \frac{V_{x_1}(\xi)}{2V(\xi)}\right)\frac{\log R}{R} + \mathcal{O}(\frac{1}{R}) \tag{36a}$$

$$B_r = \frac{V_{x_2}(\xi)R}{2V(\xi)} + \left(-\frac{\gamma\eta_t}{2} - \frac{V_{x_2}(\xi)}{2V(\xi)}\right)\frac{\log R}{R} + \mathcal{O}(\frac{1}{R}) \tag{36b}$$

$$A_i = \left(-\frac{\gamma\eta_t}{2} - \frac{V_{x_2}(\xi)}{2V(\xi)}\right)R\log R - \frac{1}{2}\Omega\eta R + \frac{\kappa\zeta_t R}{2} + \mathcal{O}(\log R) \tag{36c}$$

$$B_i = \left(\frac{\gamma\zeta_t}{2} + \frac{V_{x_1}(\xi)}{2V(\xi)}\right)R\log R + \frac{1}{2}\Omega\zeta R + \frac{\kappa\eta_t R}{2} + \mathcal{O}(\log R) \tag{36d}$$

Putting these together, we get for $R \gg 1$,

$$U_1(z,t) = e^{i\theta+S(\xi)}\left[\frac{\nabla V(\xi)z}{2V(\xi)} + \frac{i}{2}(\log R)\left(\gamma\xi_t^\perp + \frac{\nabla^\perp V(\xi)}{V(\xi)}\right)\cdot z + \frac{i}{2}\Omega\xi^\perp \cdot z + \frac{\kappa\xi_t}{2}\cdot z\right]. \tag{37}$$

Therefore, as $R \to \infty$, the asymptotic behaviour of the inner solution is given by:

$$W_0+\varepsilon W_1 = e^{i\theta+iS(\xi)}\left(\sqrt{V(\xi)}f_0(R) + \varepsilon\left[\frac{\nabla V(\xi)z}{2V(\xi)} + \frac{i}{2}(\log R)\left(\gamma\xi_t^\perp + \frac{\nabla^\perp V(\xi)}{V(\xi)}\right)\cdot z + \frac{i}{2}\Omega\xi^\perp \cdot z + \frac{\kappa\xi_t}{2}\cdot z\right]\right). \tag{38}$$

To match (38) with (19), we recall that $\tilde{x} = \frac{\varepsilon z}{\sqrt{V(\xi)}}$, $\tilde{r} = \frac{\varepsilon R}{\sqrt{V(\xi)}}$. Asymptotic matching then yields

$$\frac{i}{2}\Omega\xi^\perp + \frac{\kappa\xi_t}{2} \sim i(K + \nabla S) + \frac{i}{2}(\log\frac{\varepsilon}{\sqrt{V}})\left(\gamma\xi_t^\perp + \frac{\nabla^\perp V(\xi)}{V(\xi)}\right)$$

or

$$\gamma\xi_t^\perp - \kappa\nu\xi_t \sim \nu\left(-\Omega\xi^\perp + 2\nabla S + 2K\right) - \frac{\nabla^\perp V(\xi)}{V(\xi)}. \tag{39}$$

where $\nu = \frac{1}{\log\left(\sqrt{V(\xi)}/(\varepsilon)\right)} \sim \frac{1}{\log(1/\varepsilon)}$. The quantity K will be determined in §2.2 below through asymptotic matching, and incorporates multi-vortex interactions. In the case of a single vortex, we will show that K is bounded and thus asymptotically small compared to the other terms. In addition we recall from (14, 1b) that $\nabla S = \frac{\Omega}{2}\frac{b^2-1}{1+b^2}(\eta,\zeta)$ and $\frac{\nabla^\perp V(\xi)}{V(\xi)} = \frac{2(b^2\eta,-\zeta)}{1-\zeta^2-b^2\eta^2}$ so that (39) simplifies to

$$\gamma\xi_t^\perp - \kappa\nu\xi_t = \left(\frac{-2\Omega\nu}{1+b^2} + \frac{2}{1-\zeta^2-b^2\eta^2}\right)(-b^2\eta, \zeta) \tag{40}$$

or equivalently,

$$\gamma\xi_t + \kappa\nu\xi_t^\perp = \left(\frac{-2\Omega\nu}{1+b^2} + \frac{2}{1-\zeta^2-b^2\eta^2}\right)\begin{pmatrix} 1 & 0 \\ 0 & b^2 \end{pmatrix}\xi \tag{41}$$

8

An immediate corrollary of (41) is that a single vortex at the center $\xi = 0$ is stable if and only if $\Omega > \Omega_1$ where

$$\Omega_1 = \frac{1 + b^2}{\nu}. \tag{42}$$

As a consequence, no stable votices exist below the critical rotation rate $\Omega < \Omega_1$. The exact same critical rate was previously derived in [26] using energy methods, as well as, e.g., discussed in [38] in the context of bifurcation theory. Asymptotically, this agrees with the numerical simulations of the full PDE system (1); however, there are nontrivial corrections on this frequency that were addressed, e.g., in the work of [39].

2.2 Multiple vortices

We now look for approximate solution of (1a) with N vortices in the location ξ_j, $j = 1..N$, where all of the vortices bear the same charge $+1$. Proceeding in the same way as for a single vortex, we attempt to study the dynamics of N such vortices. The inner solution W_0 near the core of vortices is the same as for a single vortex. In the outer region, $\tilde{\phi}_0$ still satisfies the equation (10b) but with N point boundary conditions $\tilde{\phi}_0 \sim \arg(x - \xi_j)$ as $x \to \xi_j$. The singularity analysis of the outer region near ξ_j is identical to the derivation of (18) with the end result

$$\tilde{\phi}_0(\tilde{x}, t) \sim \tilde{\theta} + \frac{1}{2}(\log \tilde{r}) \left(\gamma \xi_t^\perp + \frac{\nabla^\perp V(\xi_j)}{V(\xi_j)} \right) \cdot \tilde{x} + K_j \cdot \tilde{x} \tag{43}$$

where $\tilde{x} = x - \xi_j$, $\tilde{r} = |\tilde{x}|$ with $\tilde{x} \to 0$. The multi-vortex analogue for (41) is

$$\gamma \xi_{jt} + \kappa \nu \xi_{jt}^\perp = \left(\frac{-2\Omega\nu}{1 + b^2} + \frac{2}{1 - \xi_{j1}^2 - b^2 \xi_{j2}^2} \right) \left(\begin{array}{cc} 1 & 0 \\ 0 & b^2 \end{array} \right) \xi_j - \nu 2 K_j^\perp. \tag{44}$$

It remains to determine the constants K_j via asymptotic matching. In the outer region, $\tilde{\phi}_0$ satisfies $0 \sim \Delta \tilde{\phi}_0 + \frac{\nabla V(x) \cdot \nabla \tilde{\phi}_0}{V(x)}$ or equivalently,

$$\nabla \cdot \left(V(x) \nabla \tilde{\phi}_0 \right) = 0, \tag{45a}$$

with N point-boundary conditions

$$\tilde{\phi}_0 \sim \arg(x - \xi_j) \quad \text{as} \quad x \to \xi_j, \quad j = 1 \ldots N \tag{45b}$$

In the derivation that follows, we will assume that the vortices are close to each other, separated by a small distance of $O(1/\log(1/\varepsilon))$. Similar to a computation in [14], the leading-order solution to (45) is then given by[3]

$$\nabla \tilde{\phi} \sim \sum_k \frac{V(\xi_k)}{V(x)} \nabla \arg(x - \xi_k).$$

Letting $x \to \xi_j$ we then obtain

$$\nabla \tilde{\phi} \sim \nabla \tilde{\theta} + \sum_{k \neq j} \frac{V(\xi_k)}{V(\xi_j)} \nabla \arg(\xi_k - \xi_j).$$

Matching with (43) then yields

$$K_j = \sum_{k \neq j} \frac{V(\xi_k)}{V(\xi_j)} \nabla \arg(\xi_k - \xi_j) = -\sum_{k \neq j} \frac{V(\xi_k)}{V(\xi_j)} \frac{(\xi_j - \xi_k)^\perp}{|\xi_j - \xi_k|^2}.$$

---

[3]The full solution to (45) is $\nabla \tilde{\phi} = \sum_k \frac{V(\xi_k)}{V(x)} \nabla \arg(x - \xi_k) + \frac{\nabla^\perp \psi}{V(x)}$ where ψ is chosen in such a way as to satisfy the solvability condition to make $\tilde{\phi}$ a true gradient. In particular, $\frac{\nabla^\perp \psi}{V(x)}$ is zero when V is constant. More generally, ψ satisfies $\nabla \cdot \left(\frac{\nabla \psi}{V(x)} \right) = \sum_k \nabla \left(\frac{V(\xi_k)}{V(x)} \right) \cdot \nabla^\perp \arg(x - \xi_k)$. In what follows, we assume that the vortices are close to each other in which case the term $\nabla \arg(x - \xi_k)$ dominates and ψ provides a higher-order contribution which we can ignore.

9

This yields the final result, which we summarize as follows:

$$\gamma \xi_{jt} + \nu \kappa \xi_{jt}^{\perp} \sim \left(-\frac{2\nu\Omega}{1+b^2} + \frac{2}{1 - \xi_{j1}^2 - b^2 \xi_{j2}^2} \right) \begin{pmatrix} 1 & 0 \\ 0 & b^2 \end{pmatrix} \xi_j + 2 \sum_{k \neq j} \frac{\nu(\xi_j - \xi_k)}{|\xi_j - \xi_k|^2} \frac{V(\xi_j)}{V(\xi_k)}. \tag{46}$$

This concludes the derivation of formula (2), which is the starting point for all the subsequent results of this paper. The fundamental element of novelty in our dynamical equations lies in the treatment of the interaction terms, as both the anisotropic and the dissipative cases have been recently considered in a similar vein from the viewpoint of effective particle dynamics; see, e.g., [29] and [40] for respective examples. In what follows, we will proceed to analyze the resulting systems for $N = 2$, as well as for general N number of vortices for both isotropic and anisotropic traps, comparing the conclusions to those stemming from direct numerical simulations.

3   Multi-vortex lattice density, isotropic trap.

We start by considering isotropic parabolic potential ($b = 1$) in the regime where the number of vortices N is large. As demonstrated in experiments [7, 41], in this case the vortices settle to a hexagonal "crystal lattice" configurations such as shown in Figure 1. Our goal is to estimate the asymptotic density of the resulting lattice using techniques similar to those of [27]. As a direct consequence, this computation will also yield the maximum allowed number $N_{\max}$ of vortices as a function of system parameters.

We start with the ODE system (2) that describes the evolution of multiple vortex centers. Since we are interested in the fundamental (stable equilibrium) states $\xi_j(t) \to \xi_j$, we only consider the overdamped regime (i.e. imaginary time integration) $\gamma \to \infty$. Equivalently, by rescaling the time, in the case of the isotropic potential ($b = 1$) the system (46) may be written as

$$\xi_{j\tau} = \left(-\nu\Omega + \frac{2}{1 - |\xi_j|^2} \right) \xi_j + 2\nu(1 - |\xi_j|^2) \sum_{k \neq j} \frac{\xi_k - \xi_j}{|\xi_k - \xi_j|^2} \frac{1}{1 - |\xi_k|^2}. \tag{47}$$

Being interested in the limit of large N (in which case a near "continuum of vortices" emerges) and following [27], we coarse-grain the system. This is done by defining a particle density according to:

$$\rho(x) = \sum \delta(x - \xi_k). \tag{48}$$

Equation (47) can then be written as $\xi_{j\tau} = v(\xi_j)$ where the velocity v is given by

$$v(x) = \left(-\nu\Omega + \frac{2}{1 - |x|^2} \right) x + 2\nu(1 - |x|^2) \int_{R^2} \frac{x - y}{|x - y|^2} \frac{1}{1 - |y|^2} \rho(y) dy. \tag{49a}$$

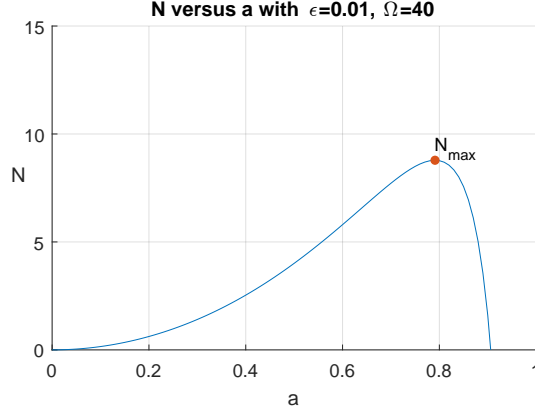In the continuum limit $N \to \infty$, this equation is coupled to the conservation of mass,

$$\rho_\tau(x, \tau) + \nabla_x \cdot (v(x)\rho(x, \tau)) = 0 \tag{49b}$$

Together, (49) describe the vortex density evolution in the limit $N \to \infty$ for the overdamped regime (47). Similarly to the analysis of [27], it can be found that the resulting steady state density ρ is compactly supported. Assuming that the density is radial, it is possible to compute the steady state $\rho(x, t) = \rho(|x|)$ and its radial support explicitly using techniques from [27], as we now show. Assume that the density is supported on a disk of radius a, so that $\rho(r) = 0$ for $r > a$ and $\rho(r) > 0$ for $0 \leq r < a$. A key identity is

$$\int_{R^2} \frac{x - y}{|x - y|^2} g(|y|) dy = x \frac{2\pi}{r^2} \int_0^r g(s)s\,ds, \tag{50}$$

which holds for any integrable function $g(r)$.

Figure 3: Number of vortices N as a function the vortex lattice radius a. Note the appearence of a maximum $N_{\max}$ corresponding to the maximum admissible number of vortices.

Applying (50) to (49a) then yields

$$v(x) = \left(-\nu\Omega + \frac{2}{1 - r^2} + \frac{4\pi\nu(1 - r^2)}{r^2} \int_0^r \frac{1}{1 - s^2}\rho(s)sds \right) x. \tag{51}$$

Inside the support $r < a$, we set $v = 0$. Upon differentiating with respect to r we obtain

$$\rho(r) = \frac{1}{4\pi\nu} \left(-\frac{2\Omega\nu r}{(1 - r^2)} - \frac{4}{1 - r^2} + \frac{8}{(1 - r^2)^2} \right). \tag{52}$$

Note from (48) that the total mass is N. Since we assumed that the density is supported on $|x| < a$, this leads to an additional constraint

$$2\pi \int_0^a \rho(s)sds = N. \tag{53}$$

Combining (52) and (53), we obtain an explicit relationship between the support radius a and N, which is given by Eq. (3).

A typical graph of N versus a is shown in Figure 3. Note that this graph attains the maximum which we compute by setting $\partial N/\partial a = 0$. This maximum $N_{\max}$ is attained at $a = \frac{\sqrt{\Omega\nu - 2}}{\sqrt{\Omega\nu + 2}}$ and has an explicit expression given by Eq. (4).

Formula (4) is one of the main results of this paper: it gives the maximum admissible number of vortices for a given rotation rate Ω. Figure 1 compares this formula (see solid curve in figure 1(b)) with both the full PDE simulations as well as the simulation of ODEs (2), from which this formula is derived.

To generate the curve "ODE", we simulated the ODE system (2), starting with $\Omega = 125$ and $N = 80$. A simple forward Euler method was found to be sufficient and was used with the stepsize $dt = 0.01$. We very gradually decreased Ω until such time that one of the particles escaped the trap (i.e. $|x_j| \geq 1$ for some j). When this occured, we decreased N by one, and recorded the corresponding Ω. The points where N drops corresponds to the "disappearence" of vortices, and are indicated by step discontinuties of the curve "ODE" in the figure. For the PDE, we simulated (1) using FlexPDE inside a disk of radius 1.3 with Dirichlet boundary conditions: $w(x) = 0$ when $|x| = 1.3$. Since the solution decays rapidly outside the trap $|x| > 1$, this radius was sufficient to discard any boundary effects (we also validated that by increasing the domain radius and ensuring that that did not affect the solution). We used the winding number of w around the contour $|x| = R$, where R is the radius chosen in such a way that $|u| < 10^{-4}$ for all $x \geq R$, to compute the number of vortices for any given snapshot. The steps in the graph correspond to values of Ω where the winding number is decreased. For both PDE and ODE computations, we made sure that Ω was decreasing

11

much slower than any transient dynamics, so that the system is in a quasi steady state, except at the points where the vortices "disappear".

We remark that the expression (4) for $N_{\max}$ is an *asymptotic* result, in the dual limit $\varepsilon \to 0$ and $N \gg 1$. In other words, it is an approximation to the true upper bound and should not be considered as an upper bound itself. In particular the crossings of "continuum" and "PDE" curves in Figure 1(b) does not contradict our results: we only claim that the curves "continuum" and "PDE" asymptote to each other for large N. On the other hand, there is a limit to the validity of the asymptotic results: if there are too many vortices, their inter-vortex distance decreases and asymptotics eventually start to fail. In practice, this imposes a restriction of how big Ω can be until the asymptotics start to fail.

It should be noted here as regards ν that its logarithmic factor involves $\log(1/\varepsilon)$, while in connection with the numerical work [39], a more accurate factor of $\log(A/\varepsilon)$ has been proposed, yielding improved agreement with the precession frequency.

It is worthwhile to also mention that Aftalion and Du [26] derived a different formula for the threshold $N_{\max}$ but using the variational framework; see formula (3.4) in [26]. In our notation, this formula can be rewritten as

$$N_{\max,\text{Aftalion/Du}} = 1 + \left(\Omega - \frac{2}{\nu} \right) \frac{1}{\log\left(2/\nu\right)}. \tag{54}$$

It is also shown in Figure 1. Unlike our formula (54) is linear in Ω and while reasonably accurate for a small number of vortices, it becomes progressively less acurate for large Ω.

Finally, let us mention that a similar computation was done in [27] for a simplified version of the vortex equations of motion that did not incorporate the trap density in vortex-to-vortex interactions suggested in [17], namely

$$z_{j\tau} = \left(-\nu\Omega + \frac{2}{1 - |z_j|^2} \right) z_j + 2\nu \sum_{k \neq j} \frac{z_k - z_j}{|z_k - z_j|^2}. \tag{55}$$

For this simplified system, a similar analysis (see [27], section 4) yields the formula

$$N_{\max,\text{CKK}} = \frac{1}{\nu} \left(\sqrt{\frac{\Omega\nu}{2}} - 1 \right)^2. \tag{56}$$

In fact, formulas (4) and (56) both agree near $\Omega\nu = 2$ as can be seen by expanding in Taylor series around $\Omega\nu = 2$; in this regime, $\nu N_{\max}$ is small, the radius a is also small and both formulas yield $\nu N_{\max} = \frac{1}{16}(\Omega\nu - 2)^2 + O((\Omega\nu - 2)^3)$ with $a \sim \sqrt{\Omega\nu - 2} + o(\sqrt{\Omega\nu - 2})$. However the two deviate significantly for larger values of N.

4   Two vortices, anisotropic trap

Let us now investigate in some more detail the case of two vortices in an anisotropic trap ($b \neq 1$). In the isotropic case ($b = 1$), a basic steady state configuration consists of two antipodal vortices along *any* line through the center due to the rotational invariance of the model. It should be highlighted, however, that the work of [17, 18] revealed that this configuration is only stable within a range of distances of the antipodal pair from the origin. Beyond a critical threshold, the energetically favored state becomes an asymmetric one. On the other hand, even for the antipodal states, the introduction of the anisotropy breaks the rotational symmetry, leading to two possible steady states: either vortex centers lie on the x-axis or on the y-axis. Both configurations may be admissible as steady states. However the stability analysis below will show that only the configuration with two vortices along the longest axis of the ellipse $x^2 + by^2 = 1$ is stable, the other configuration being unstable. This is in line with earlier works in the case of oppositely charged vortices; see, e.g., [28].

First, consider two votices in a stable configuration along the x-axis, with coordinates $\xi_1 = (r, 0)$ and $\xi_2 = (-r, 0)$. Upon substituting into the equation of motion (2) we obtain an algebraic equation for r,

$$\left(-\frac{\nu\Omega}{1+b^2} + \frac{1}{1-r^2} \right) r + \frac{\nu}{2r} = 0. \tag{57}$$

This equation is quadratic in r^2, and admits two positive solutions $r_\pm$ with $r_- < r_+$, provided that $\Omega > \Omega_2$ where

$$\Omega_2 = \frac{1}{\nu} \frac{1+b^2}{2} \left(\sqrt{2} + \sqrt{\nu} \right)^2. \tag{58}$$

There is a fold point at $\Omega = \Omega_2$ and the solution disappears when $\Omega < \Omega_2$. This was already observed in the work of [17] in the case of an isotropic trap. Note that to leading order in ν, $\Omega_2 \sim (1+b^2)/\nu$, which agrees with the stability threshold for a single spike Ω_1, see (42). We also remark that the same formula for Ω_2 holds for two vortices along the $y-$axis. This can be seen as follows: assume that the equilibrium is at $(0, \pm\hat{r})$. By rescaling $\hat{r} = r/b$, we find that r then satisfies (57), so that the fold point Ω_2 is the same whether the vortices are along $x-$ or $y-$ axis.

In the pioneering work [26], Aftalion and Du derived a slightly different formula for Ω_2, using a related energy method, see formula (22) there. Written in our notation, the formula in [26] reads:

$$\Omega_{2,\text{Aftalion/Du}} = \frac{1+b^2}{\nu} + \frac{1+b^2}{2} \log \left(\frac{1+b^2}{\nu} \right). \tag{59}$$

While both formulae have the same leading-order behaviour in ν, they have very different (and large) correction terms. Figure 4(a) shows a direct comparison between (58), (59) and the full numerical simulations of the PDE (1). Formula (58) appears to be a significant improvement over (59).

For $\Omega > \Omega_2$, the only *potentially stable* solution is the one corresponding to r_- as can be seen by considering perturbations along the $x-$axis. However this does not tell the whole story: a solution may exist and be stable along the x-axis, but be unstable with respect to the full spectrum of two-dimensional perturbations. To describe the full stability, as in section 3, we will – for simplicity – consider the overdamed system $\kappa = 0, \gamma = 1$ (it can be shown that stability properties are independent of κ as long as $\gamma > 0$). The full equations then become

$$\frac{dx_1}{dt} = \left(-2\hat{\Omega} + \frac{2}{1-x_1^2-b^2y_1^2} \right) x_1 + \frac{2\nu(x_1-x_2)}{(x_1-x_2)^2+(y_1-y_2)^2} \frac{1-x_1^2-b^2y_1^2}{1-x_2^2-b^2y_2^2}$$

$$\frac{dy_1}{dt} = \left(-2\hat{\Omega} + \frac{2}{1-x_1^2-b^2y_1^2} \right) b^2y_1 + \frac{2\nu(y_1-y_2)}{(x_1-x_2)^2+(y_1-y_2)^2} \frac{1-x_1^2-b^2y_1^2}{1-x_2^2-b^2y_2^2}$$

$$\frac{dx_2}{dt} = \left(-2\hat{\Omega} + \frac{2}{1-x_2^2-b^2y_2^2} \right) x_2 + \frac{2\nu(x_2-x_1)}{(x_1-x_2)^2+(y_1-y_2)^2} \frac{1-x_2^2-b^2y_2^2}{1-x_1^2-b^2y_1^2} \tag{60}$$

$$\frac{dy_2}{dt} = \left(-2\hat{\Omega} + \frac{2}{1-x_2^2-b^2y_2^2} \right) b^2y_2 + \frac{2\nu(y_2-y_1)}{(x_1-x_2)^2+(y_1-y_2)^2} \frac{1-x_2^2-b^2y_2^2}{1-x_1^2-b^2y_1^2}$$

where we defined

$$\hat{\Omega} := \frac{\nu\Omega}{1+b^2}. \tag{61}$$

Linearizing around the equilibrium $x_1 = r, x_2 = -r, \ y_1 = y_2 = 0$, we obtain the following Jacobian matrix,

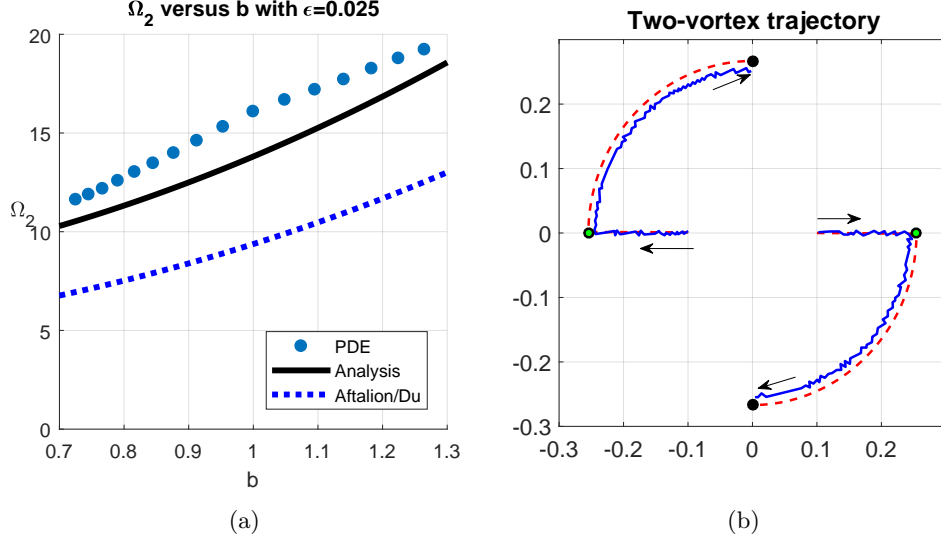$$\begin{pmatrix} M_1 & 0 & M_3 & 0 \\ 0 & M_2 & 0 & M_4 \\ M_3 & 0 & M_1 & 0 \\ 0 & M_4 & 0 & M_2 \end{pmatrix}$$

Figure 4: (a) Ω_2 (the critical rotation rate beyond which dipole solutions can be identified in an anisotropic trap) as a function of anisotropy parameter b : comparison of full numerics and asymptotics. Dots are obtained from the full numerical computations of the PDE (1). The solid line denotes the asymptotic formula (58). The dashed line is the formula (59) derived in [26]. Parameter values are $\gamma = 1$, $\kappa = 0$, $\varepsilon = 0.025$. (b) Two-vortex trajectory. Parameter values are $\varepsilon = 0.025$, $\Omega = 22.133$ and $b = 0.9535$. Initial conditions consist of two vortices along x-axis. The arrows indicate the direction of motion. At first, the vortices approach a saddle point along the x-axis (indicated by green-black dots). But eventually the two vortices settle along the $y-$axis (indicated by black dots). Solid curve shows vortex centers from the full PDE simulation of (1) with $\gamma = 1, \kappa = 0$. Dashed line shows the simulation of the reduced ODE (60).

where

$$M_1 = -2\hat{\Omega} + \frac{2}{1-r^2} + \frac{4r^2}{(1-r^2)^2} - \frac{\nu}{2r^2} - \frac{2\nu}{1-r^2}, \qquad M_2 = -2\hat{\Omega}b^2 + \frac{2b^2}{1-r^2} + \frac{\nu}{2r^2}$$

$$M_3 = \frac{\nu}{2r^2} - \frac{2\nu}{1-r^2}, \qquad M_4 = -\frac{2\nu}{r^2}$$

The eigenvalues of this matrix are easily computed as $M_1 \pm M_3$ and $M_2 \pm M_4$ which yields,

$$\lambda_1 = M_1 + M_3 = -2\hat{\Omega} + \frac{2}{1-r^2} + \frac{4r^2}{(1-r^2)^2} - \frac{4\nu}{1-r^2} \qquad \lambda_2 = M_1 - M_3 = -2\hat{\Omega} + \frac{2}{1-r^2} + \frac{4r^2}{(1-r^2)^2} - \frac{2\nu}{r^2}$$

$$\lambda_3 = M_2 + M_4 = -2\hat{\Omega}b^2 + \frac{2b^2}{1-r^2}, \qquad \lambda_4 = M_2 - M_4 = -2\hat{\Omega}b^2 + \frac{2b^2}{1-r^2} + \frac{\nu}{r^2}.$$

Using the relationships $\hat{\Omega} = \frac{\nu}{2r^2} + \frac{1}{1-r^2}$ and $\Omega > \Omega_2$, basic algebra shows that $\lambda_{1,2,3} \leq 0$. On the other hand, λ_4 becomes

$$\lambda_4 = 2(-b^2 + 1)\frac{\nu}{r^2}$$

and goes through zero precisely at $b = 1$; it is stable for $b > 1$ and unstable for $0 < b < 1$. The underlying elliptic trap has the form $x^2 + b^2y^2 = 1$. When $b > 1$, the x-axis is the major axis and the y-axis is the minor axis of the ellipse; the opposite is true for $b < 1$. This shows that the two-vortex configuration is stable only along the *major* axis.

Figure 4(b) illustrates this stability result. There, we took $b = 0.9535$, so that the trap is nearly circular but with the extent of the condensate along the $y-$axis being slightly longer. So we expect a two-vortex
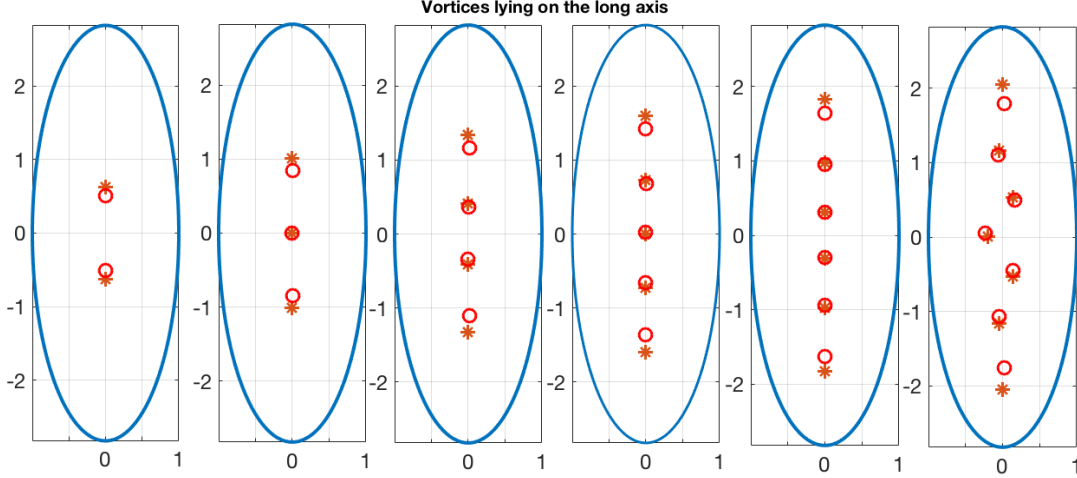
14

Figure 5: Comparison of the steady state of PDE and ODE simulations for $N = 2 \ldots 7$ vortices. '$*$' denotes the steady state of the ODE system (2) whereas 'o' is from the PDE system (1). The parameters are chosen as: $\gamma = 1$, $\kappa = 0$, $b = \frac{1}{\sqrt{8}}$, $\varepsilon = 0.025$, $\Omega = 6.72$ for two vortices and $\Omega = 7.21$ for three to seven vortices. The boundary of the elliptical trap $x^2 + b^2 y^2 = 1$ is also shown.

equilibrium to be unstable along the $x-$axis but stable along the $y-$axis. This is indeed what happens. We ran the imaginary-time integration ($\kappa = 0$) for the full PDE (1), starting with initial conditions consisting of two vortices along the $x-$axis. At first, the two vortices approach the unstable equilibrium along the x-axis (although unstable, it is a saddle point and initial conditions are along its stable manifold). However eventually, since this equilibrium is unstable, they travel towards a stable equilibrium along the $y-$axis.

5   Large N limit with strongly anisotropic trap

We now consider the strongly anisotropic parabolic potential case of small [4] b. Figure 5 illustrates this case with $b = \frac{1}{\sqrt{8}}$. For sufficiently strong anisotropy, the vortices align along the major axis of the elliptic trap (the y-axis in the case $b \to 0$); see, e.g., also the work of [28] for oppositely charged vortices. Exactly *how* strong depends on the number of vortices and the exact dependence is an open question that we leave for future study. For now, we simply assume that the anisotropy is sufficiently strong for the full alignment to occur, so that the steady state is effectively one-dimensional. In this case, the ODE system (2) reduces motion purely along the $y-$axis, leading to the following dynamical system of N variables:

$$y_{jt} = \left(-2\hat{\Omega} + \frac{2}{1 - b^2 y_j^2}\right) y_j + 2\nu \sum_{k \neq j} \frac{1 - b^2 y_j^2}{1 - b^2 y_k^2} \frac{y_j - y_k}{|y_j - y_k|^2}, \tag{62a}$$

where

$$\hat{\Omega} := \nu \frac{\Omega}{1 + b^2}. \tag{62b}$$

---

[4]Notice that for large b, the width of the ellipse $x^2 + b^2 y^2 = 1$ is of $O(1/b)$. Since the size of the vortex core is of $O(\varepsilon)$, asymptotics require that $b \ll O(1/\varepsilon)$ (otherwise the vortex size is comparable to the domain size, in which case asymptotics break down). For this reason, we take the limit $b \to 0$ (high anisotropy along the y-axis) rather than $b \to \infty$ (high anisotropy along the x-axis).

15

(where for simplicity we took the overdamped limit $\gamma = 1, \kappa = 0$). Define $z_j = by_j$ so that (62a) becomes

$$\frac{1}{b^2}z_{jt} = \left(-2\hat{\Omega} + \frac{2}{1 - z_j^2}\right)z_j + 2\nu\sum_{k\neq j}\frac{1 - z_j^2}{1 - z_k^2}\frac{z_j - z_k}{|z_j - z_k|^2}.$$

We wish to compute the effective one-dimensional density of the resulting steady state in the continuum limit $N \to \infty$ of this system. As in §3, we define the one-dimensional density to be

$$\rho(z) = \sum \delta(z - z_j).$$

The steady-state density then satisfies

$$\left(-\hat{\Omega} + \frac{1}{1 - z^2}\right)z + \nu\left(1 - z^2\right)\fint_{-a}^{a}\frac{1}{y - z}\frac{1}{1 - y^2}\rho(y)dy = 0 \tag{63a}$$

where $\fint_{-a}^{a}$ denotes the Cauchy principal value integral. Here, a is the radius of the one-dimensional vortex "lattice". The solution to (63a) is subject to the additional mass constraint

$$\int_{-a}^{a}\rho(z)dz = N \tag{63b}$$

Together, equations (63) are to be solved for both the density $\rho(z)$ and the radius a.

A solution to (63) can be derived using techniques involving the Chebychev polynomials, as suggested by [42], see Chapter 18 there (the Fourier–Chebyshev series). We start by recalling the following standard identities between Chebyshev polynomials U_n and T_n:

$$\fint_{-1}^{1}\frac{\sqrt{1 - y^2}U_{n-1}(x)}{y - x}dy = -\pi T_n(x) \tag{64a}$$

$$\fint_{-1}^{1}\frac{T_{n(x)}}{(y - x)\sqrt{1 - y^2}}dy = \pi U_{n-1}(x) \tag{64b}$$

$$\fint_{-1}^{1}\frac{T_n(x)T_m(x)}{\sqrt{1 - y^2}}dy = \begin{cases} 0 & n \neq m \\ \pi & n = m = 0 \\ \pi/2 & n = m \neq 0 \end{cases} \tag{64c}$$

$$\fint_{-1}^{1}U_n(x)U_m(x)\sqrt{1 - y^2}dy = \begin{cases} 0 & n \neq m \\ \pi/2 & n = m = 0 \end{cases}. \tag{64d}$$

Identity (64a) as well as the form of the integral equation (63a) motivates the following anzatz for the density ρ:

$$\rho(z) = -\frac{1}{\pi}\sum_{i=1}^{\infty}c_iU_{i-1}(\frac{z}{a})\left(1 - z^2\right)\sqrt{1 - \frac{z^2}{a^2}}. \tag{65a}$$

Using (64d) in Eq. (63a) then yields the following expression for c_i in terms of a:

$$c_i = \frac{2}{\pi}\int_{-1}^{1}\left(-\hat{\Omega} + \frac{1}{1 - a^2y^2}\right)\frac{ay}{\nu\left(1 - a^2y^2\right)}T_i(y)\frac{1}{\sqrt{1 - y^2}}dy. \tag{65b}$$

Upon substituting (65a) into (63a) and using identities (64) we obtain

$$\int_{-a}^{a}\rho(z)dz = -\frac{a}{2}\left(c_1(1 - \frac{a^2}{4}) - \frac{a^2}{4}c_3\right) = N \tag{65c}$$
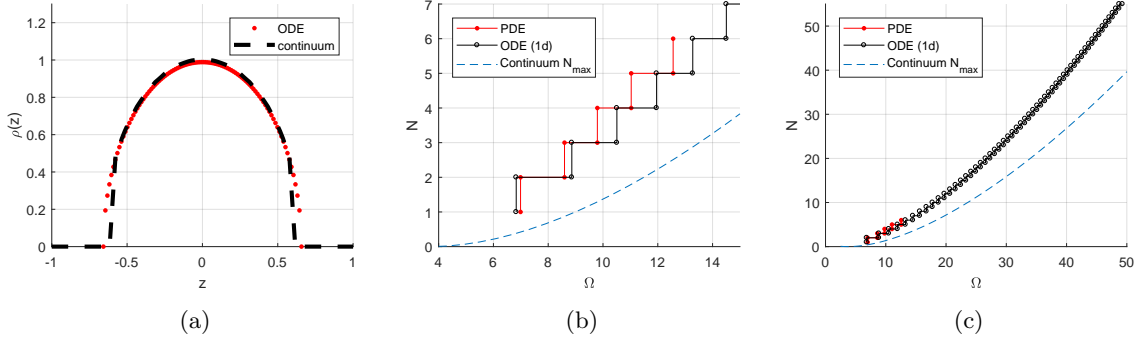
16

Figure 6: (a) Steady state density of the ODE system (62), compared with the continuum limit (65), where only eight terms of the series is used. Here, $N = 40$ and $\hat{\Omega} = 40$ (b) Maximal admissible number of vortices for the full PDE simulation of (1) versus the ODE system (62), versus the versus continuum formula (66). Parameters are $\gamma = 1, \kappa = 0, \varepsilon = 0.025$, $b = \frac{1}{\sqrt{8}}$ and Ω is slowly decreasing according to the formula $\Omega = 10 - 10^{-4}t$. (c) Comparison of the ODE (62) and continuum limit formula (66) with ODE motion restricted to the y-axis, for larger number of vortices. Same parameters as in (b), except that $\Omega = 60 - 10^{-4}t$.

Evaluating c_1 and c_3 using (65b) finally yields the following relationship between N and a,

$$N = \frac{1}{\nu}\left(\frac{\hat{\Omega}a^2}{2\sqrt{1-a^2}} - \frac{(a^2-2)^2}{\nu(1-a^2)^{\frac{3}{2}}} + 1\right). \tag{65d}$$

Note that while the expression for the radius a is explicit, the density $\rho(z)$ itself does not appear to have a closed form solution, having an infinite-series representation (65a). However the coefficients c_i in (65a) are easy to compute numerically, while in practice the series representation converges very quickly. Figure 6(a) shows a direct comparison between the analytical density (65a) and the steady state of (63) with $N = 40$, verifying that the analytical prediction is in very good agreement with the numerical ODE result.

The function $a \to N(a)$ has a unique maximum at $a^2 = 2\left(\hat{\Omega} - 1\right)/(2\hat{\Omega} + 1)$, given by

$$N_{\mathrm{max,1d}} = \frac{1}{\nu}\left(1 + 3^{-3/2}(\hat{\Omega} - 4)\sqrt{1 + 2\hat{\Omega}}\right). \tag{66}$$

This provides the asymptotic upper bound for the number of vortices that can be aligned along the x-axis. This is the main result of this section, concluding the derivation of (6). Figure 6(c) shows the comparison between the formula (66) and the ODE. Although it appears that the two curves diverge, their ratio approaches 1 as $\hat{\Omega}$ is increased; a similar comparison but for small values of Ω is shown in Fig. 6(b).

6 Discussion

In this paper we derived a novel and more accurate set of ODEs (2) for vortex motion in BEC with an (isotropic, as well as with an) anisotropic trap. These ODEs incorporate the effect of the trap inhomogenuity on vortex-to-vortex interactions. In turn, the analysis of ODEs yields an accurate analytical formula for the vortex lattice density, as well as the maximal admissible number of vortices N_{max} as a function of rotation rate Ω under two scenarios: isotropic trap with large N, and high-anisotropy regime with large N. Additionally, we examined existence and stability of two vortices in an anisotropic trap; i.e., we focused both on the fundamental building block of the inter-vortex interactions and the large N "vortex crystal" limit. For the isotropic case, we used techniques from swarming literature [27, 43] to estimate the large-N vortex lattice
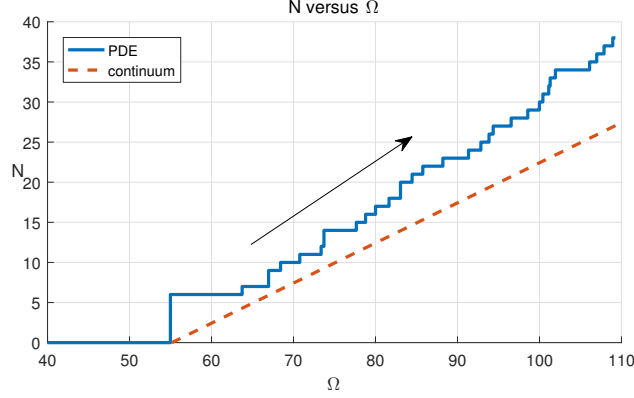
17

Figure 7: Number of vortices as a function of very slowly increasing $\Omega : \Omega = 10^{-2}t$. All other parameters are as in Figure 1. The curve "PDE" is from PDE simulations whereas the curve "continuum" is the asymptotic estimate (67).

density. In the case of high-anisotropy, we used Chebychev expansions to explicitly compute the critical thresholds and analyze the vortex density.

It would be interesting to redo the analysis in [17] for the new ODE system (2). For example, it would be relevant to identify in that context the asymmetric configurations of two vortices, as well as to extend considerations beyond the case of two, i.e., to triplets of vortices, as well as beyond.

Our results improve upon known results in the literature in two ways. The reduced system of motion (2) is more accurate than previously reported in e.g. [17, 27] (see [4] for a relevant discussion of earlier models). As a consequence, we have obtained more accurate thresholds for existence and stability, especially in the case of multiple vortices, but also in the case of two vortices within an anisotropic trap. Numerical experiments show that these thresholds improve also upon those found in [26], for example.

It is interesting to note that that in addition to the upper bound $N_{\max}$, there is also a lower bound on the number of vortices, $N_{\min}$, for a given rotation rate Ω. As Ω is sufficiently increased, vortices spontaneously nucleate from the Thomas-Fermi boundary. In the case of an isotropic trap, a zero-vortex state becomes unstable as Ω increases past $\underline{\Omega} \sim 2.561\varepsilon^{-2/3}$ – see [44, 45, 46] for derivation. This computation can be extended to a single vortex at the center of degree N. In this case, one finds that the stability threshold is $\underline{\Omega} \sim 2.53\varepsilon^{-2/3} + 2N$. Solving for N, this in turn yields the formula

$$N_{\min} \sim \frac{\Omega}{2} - 1.28\varepsilon^{-2/3}. \tag{67}$$

Speculatively, let us now make a very crude approximation, and naïvely assume that the entire vortex lattice of N vortices can be approximated by a single vortex of degree N at the origin. This assumption is clearly incorrect if the vortex lattice occupies the entire trap, but may be reasonable if we suppose that the entire vortex lattice is clustered near the center and away from the Thomas-Fermi boundary. In any case, under this very crude assumption, (67) provides an asymptotic approximation to the *lower bound* for existence of N vortices as a function of Ω, so that $N_{\min} < N < N_{\max}$. Surprisingly, this actually works relatively well in practice, at least for relatively small vortex numbers as Figure 7 illustrates. An open question is to extend this bound to an anisotropic trap, as well as the situation where the vortex lattice is spread throughout the trap, and cannot be easily reduced to a single $N-$degree vortex.

In conclusion, direct asymptotic reduction of the GPE, combined with coarse-graining techniques for large number of vortices (and bifurcation analysis for small N vortex clusters) provide a powerful set of tools that yields novel insights into a well-studied classical problem of Bose-Einstein Condensates.

References

[1] Y. Castin, R. Dum, Bose-einstein condensates with vortices in rotating traps, The European Physical Journal D-Atomic, Molecular, Optical and Plasma Physics 7 (3) (1999) 399–412.

[2] A. L. Fetter, Rotating trapped bose-einstein condensates, Reviews of Modern Physics 81 (2) (2009) 647.

[3] A. Aftalion, Vortices in Bose-Einstein Condensates, Vol. 67, Springer Science & Business Media, 2007.

[4] P. Kevrekidis, D. Frantzeskakis, R. Carretero-Gonzlez, The Defocusing Nonlinear Schrdinger Equation, Society for Industrial and Applied Mathematics, Philadelphia, PA, 2015. `arXiv:http://epubs.siam.org/doi/pdf/10.1137/1.9781611973945`, `doi:10.1137/1.9781611973945`.
URL `http://epubs.siam.org/doi/abs/10.1137/1.9781611973945`

[5] E. H. Lieb, R. Seiringer, J. Yngvason, A rigorous derivation of the gross–pitaevskii energy functional for a two-dimensional bose gas, Communications in Mathematical Physics 224 (1) (2001) 17–31.

[6] E. H. Lieb, R. Seiringer, Derivation of the gross-pitaevskii equation for rotating bose gases, Communications in mathematical physics 264 (2) (2006) 505–537.

[7] J. Abo-Shaeer, C. Raman, J. Vogels, W. Ketterle, Observation of vortex lattices in bose-einstein condensates, Science 292 (5516) (2001) 476–479.

[8] K. Madison, F. Chevy, W. Wohlleben, J. Dalibard, Vortex formation in a stirred bose-einstein condensate, Physical Review Letters 84 (5) (2000) 806.

[9] S. Serfaty, On a model of rotating superfluids, ESAIM: Control, Optimisation and Calculus of Variations 6 (2001) 201–238.

[10] R. Ignat, V. Millot, The critical velocity for vortex existence in a two-dimensional rotating bose–einstein condensate, Journal of Functional Analysis 233 (1) (2006) 260–306.

[11] R. Ignat, V. Millot, Energy expansion and vortex location for a two-dimensional rotating bose–einstein condensate, Reviews in Mathematical Physics 18 (02) (2006) 119–162.

[12] V. Bretin, S. Stock, Y. Seurin, J. Dalibard, Fast rotation of a bose-einstein condensate, Physical review letters 92 (5) (2004) 050403.

[13] V. Schweikhard, I. Coddington, P. Engels, V. Mogendorff, E. A. Cornell, Rapidly rotating bose-einstein condensates in and near the lowest landau level, Physical review letters 92 (4) (2004) 040404.

[14] D. E. Sheehy, L. Radzihovsky, Vortices in spatially inhomogeneous superfluids, Physical Review A 70 (6) (2004) 063620.

[15] D. E. Sheehy, L. Radzihovsky, Vortex lattice inhomogeneity in spatially inhomogeneous superfluids, Physical Review A 70 (5) (2004) 051602.

[16] M. Correggi, N. Rougerie, Inhomogeneous vortex patterns in rotating bose-einstein condensates, Communications in Mathematical Physics 321 (3) (2013) 817–860.

[17] R. Navarro, R. Carretero-González, P. Torres, P. Kevrekidis, D. Frantzeskakis, M. Ray, E. Altuntaş, D. Hall, Dynamics of a few corotating vortices in bose-einstein condensates, Physical review letters 110 (22) (2013) 225301.

[18] A. V. Zampetaki, R. Carretero-González, P. G. Kevrekidis, F. K. Diakonos, D. J. Frantzeskakis, Exploring rigidly rotating vortex configurations and their bifurcations in atomic bose-einstein condensates, Phys. Rev. E 88 (2013) 042914. `doi:10.1103/PhysRevE.88.042914`.
URL `https://link.aps.org/doi/10.1103/PhysRevE.88.042914`

[19] E. Weinan, Dynamics of vortices in ginzburg-landau theories with applications to superconductivity, Physica D: Nonlinear Phenomena 77 (4) (1994) 383–404.

[20] R. Jerrard, D. Smets, Vortex dynamics for the two-dimensional non-homogeneous gross-pitaevskii equation, Ann. Sc. Norm. Sup. Pisa 14 (2015) 729–766.

[21] D. E. Pelinovsky, P. G. Kevrekidis, Variational approximations of trapped vortices in the large-density limit, Nonlinearity 24 (4) (2011) 1271.
URL http://stacks.iop.org/0951-7715/24/i=4/a=013

[22] FlexPDE6, PDE Solutions Inc. URL http://www.pdesolutions.com.

[23] M. Tsubota, K. Kasamatsu, M. Ueda, Vortex lattice formation in a rotating bose-einstein condensate, Physical Review A 65 (2) (2002) 023603.

[24] A. Penckwitt, R. Ballagh, C. Gardiner, Nucleation, growth, and stabilization of bose-einstein condensate vortex lattices, Physical review letters 89 (26) (2002) 260402.

[25] D. L. Feder, C. W. Clark, B. I. Schneider, Vortex stability of interacting bose-einstein condensates confined in anisotropic harmonic traps, Physical review letters 82 (25) (1999) 4956.

[26] A. Aftalion, Q. Du, Vortices in a rotating bose-einstein condensate: Critical angular velocities and energy diagrams in the thomas-fermi regime, Physical Review A 64 (6) (2001) 063603.

[27] T. Kolokolnikov, P. Kevrekidis, R. Carretero-González, A tale of two distributions: from few to many vortices in quasi-two-dimensional bose–einstein condensates, The Royal Society 470 (2168) (2014) 20140048.

[28] J. Stockhofe, S. Middelkamp, P. G. Kevrekidis, P. Schmelcher, Impact of anisotropy on vortex clusters and their dynamics, EPL (Europhysics Letters) 93 (2) (2011) 20008.
URL http://stacks.iop.org/0295-5075/93/i=2/a=20008

[29] R. H. Goodman, P. G. Kevrekidis, R. Carretero-Gonzlez, Dynamics of vortex dipoles in anisotropic bose–einstein condensates, SIAM Journal on Applied Dynamical Systems 14 (2) (2015) 699–729. arXiv:
https://doi.org/10.1137/140992345, doi:10.1137/140992345.
URL https://doi.org/10.1137/140992345

[30] S. McEndoo, T. Busch, Small numbers of vortices in anisotropic traps, Physical Review A 79 (5) (2009) 053616.

[31] J.-k. Kim, A. L. Fetter, Dynamics of a single ring of vortices in two-dimensional trapped bose-einstein condensates, Physical Review A 70 (4) (2004) 043624.

[32] K. Kasamatsu, M. Tsubota, M. Ueda, Vortices in multicomponent bose–einstein condensates, International Journal of Modern Physics B 19 (11) (2005) 1835–1904.

[33] A. A. Svidzinsky, A. L. Fetter, Dynamics of a vortex in a trapped bose-einstein condensate, Physical Review A 62 (6) (2000) 063617.

[34] A. A. Svidzinsky, A. L. Fetter, Stability of a vortex in a trapped bose-einstein condensate, Physical review letters 84 (26) (2000) 5919.

[35] L. Pismen, J. Rubinstein, Motion of vortex lines in the ginzburg-landau model, Physica D: Nonlinear Phenomena 47 (3) (1991) 353–360.

[36] B. Rubinstein, L. Pismen, Vortex motion in the spatially inhomogenous conservative ginzburg-landau model, Physica D: Nonlinear Phenomena 78 (1-2) (1994) 1–10.

[37] F. Bethuel, H. Brezis, F. Hélein, Ginzburg-Landau Vortices, Vol. 13, Springer Science & Business Media, 2012.

[38] D. E. Pelinovsky, P. G. Kevrekidis, Bifurcations of asymmetric vortices in symmetric harmonic traps, Applied Mathematics Research eXpress 2013 (1) (2013) 127.

[39] S. Middelkamp, P. G. Kevrekidis, D. J. Frantzeskakis, R. Carretero-González, P. Schmelcher, Bifurcations, stability, and dynamics of multiple matter-wave vortex states, Phys. Rev. A 82 (2010) 013646. `doi:10.1103/PhysRevA.82.013646`.
URL `https://link.aps.org/doi/10.1103/PhysRevA.82.013646`

[40] D. Yan, R. Carretero-González, D. J. Frantzeskakis, P. G. Kevrekidis, N. P. Proukakis, D. Spirn, Exploring vortex dynamics in the presence of dissipation: Analytical and numerical results, Phys. Rev. A 89 (2014) 043613. `doi:10.1103/PhysRevA.89.043613`.
URL `https://link.aps.org/doi/10.1103/PhysRevA.89.043613`

[41] C. Raman, J. Abo-Shaeer, J. Vogels, K. Xu, W. Ketterle, Vortex nucleation in a stirred bose-einstein condensate, Physical review letters 87 (21) (2001) 210402.

[42] Y. V. Shestopalov, Y. G. Smirnov, Integral equations, Karlstad University, Karlstad, 2002.

[43] R. C. Fetecau, Y. Huang, T. Kolokolnikov, Swarm dynamics and equilibria for a nonlocal aggregation model, Nonlinearity 24 (10) (2011) 2681.

[44] J. Anglin, Local vortex generation and the surface mode spectrum of large bose-einstein condensates, Physical review letters 87 (24) (2001) 240401.

[45] R. Carretero-González, P. G. Kevrekidis, T. Kolokolnikov, Vortex nucleation in a dissipative variant of the nonlinear schrödinger equation under rotation, Physica D: Nonlinear Phenomena 317 (2016) 1–14.

[46] J. C. Tzou, P. G. Kevrekidis, T. Kolokolnikov, R. Carretero-Gonzalez, Weakly nonlinear analysis of vortex formation in a dissipative variant of the gross–pitaevskii equation, SIAM Journal on Applied Dynamical Systems 15 (2) (2016) 904–922.